Mathematical Biosciences and Engineering

MBE, 19(12): 11821–11839.
DOI: 10.3934/mbe.2022551
Received: 18 May 2022
Revised: 01 August 2022
Accepted: 03 August 2022
Published: 16 August 2022

http://www.aimspress.com/journal/MBE

Research article

Risk stratification of acute myeloid leukemia: Assessment using a novel prediction model based on ferroptosis-immune related genes

Xing Guo and Xiaogang Zhou*

Department of Hematology, The Fourth Affiliated Hospital of Nanjing Medical University, Nanjing 210000, China

* **Correspondence:** Email: battistuta007@163.com; Tel: +8615996226022.

Abstract: In acute myeloid leukemia (AML), the link between ferroptosis and the immune microenvironment has profound clinical significance. The objective of this study was to investigate the role of ferroptosis-immune related genes (FIRGs) in predicting the prognosis and therapeutic sensitivity in patients with AML. Using The Cancer Genome Atlas dataset, single sample gene set enrichment analysis was performed to calculate the ferroptosis score of AML samples. To search for FIRGs, differentially expressed genes between the high- and low-ferroptosis score groups were identified and then cross-screened with immune related genes. Univariate Cox and LASSO regression analyses were performed on the FIRGs to establish a prognostic risk score model with five signature FIRGs (*BMP2, CCL3, EBI3, ELANE*, and *S100A6*). The prognostic risk score model was then used to divide the patients into high- and low-risk groups. For external validation, two Gene Expression Omnibus cohorts were employed. Overall survival was poorer in the high-risk group than in the low-risk group. The novel risk score model was an independent prognostic factor for overall survival in patients with AML. Infiltrating immune cells were also linked to high-risk scores. Treatment targeting programmed cell death protein 1 may be more effective in high-risk patients. This FIRG-based prognostic risk model may aid in optimizing prognostic risk stratification and treatment of AML.

Keywords: acute myeloid leukemia; ferroptosis; immune microenvironment; single sample gene set enrichment analysis; immunotherapy

Abbreviations: AML: Acute myeloid leukemia; ATP: Adenosine triphosphate; AUC: Area under the curve; BM: Bone marrow; BMP2: Bone morphogenetic protein 2; BP: Biological processes; CC:

Cellular components; CCL3: C-C motif chemokine ligand 3; CNS: central nervous system; CR: complete remission; DCA: Decision curve analysis; DEGs: Differentially expressed genes; EBI3: Epstein-Barr Virus Induced 3; ELANE: Elastase: neutrophil expressed; FAB: French-American-British; FC: Fold change; FIRGs: Ferroptosis–immune related genes; GDSC: Genomics of Drug Sensitivity in Cancer; GEO: Gene Expression Omnibus; GO: Gene Ontology; GSEA: Gene set enrichment analysis; IC50: Half-maximal inhibitory concentration; IL: Interleukin; KEGG: Kyoto Encyclopedia of Genes and Genomes; K-M: Kaplan-Meier; LASSO: least absolute shrinkage and selection operator; MAPK: Mitogen-activated protein kinase; MF: Molecular function; NF-κB: Nuclear factor kappa B; NS: Not significant; OS: overall survival; PD1: Programmed cell death protein 1; RCD: regulated cell death; ROC: Receiver operating characteristic; S100A6: S100 calcium binding protein A6; SHP2: SH2 containing protein-tyrosine phosphatase-2; ssGSEA: Single sample gene set enrichment analysis; TCGA: The Cancer Genome Atlas; TNF: Tumor necrosis factor; t-SNE: t-distributed stochastic neighbor embedding; PCA: principal component analysis; EDA: exploratory data analysis; IDI: Integrated discrimination improvement analysis

1. Introduction

Traditional treatment strategies for acute myeloid leukemia (AML) include intensive chemotherapy, hypomethylating medications, and hematopoietic stem cell transplantation. The 5-year overall survival (OS) rate remains poor, at no more than 30% [1]. Strategies for AML treatment have recently evolved away from traditional therapies toward immunotherapy and targeted therapy. However, more than half of the patients still experience relapse or become treatment refractory. The median OS for these patients is only 0.5 years [2]. It is therefore critical to find a more accurate prognostic risk stratification that can assist in accurately identifying patients who will respond to specific treatments.

Ferroptosis is a modulated form of cell death involving iron overload and the overproduction of reactive oxygen species [3]. Activation of ferroptosis triggers the death of oncocytes, especially in cancers resistant to traditional treatment [4–6]. Although the precise effects and mechanisms of ferroptosis in the pathogenesis of AML remain unclear, some studies have shown that patients with AML frequently exhibit abnormal expression of ferroptosis-associated genes. Promoting ferroptosis in AML cells through treatment with the multikinase inhibitor sorafenib could help in reversing the drug resistance of tumor cells [7,8]. This suggests that ferroptosis could be used as a new indicator for AML risk stratification.

Immunotherapy, including antibody-based treatment, tumor vaccines, immune checkpoint inhibitors, and adoptive cellular immunotherapy, has shown great clinical application prospects for AML [9]. However, research on immunotherapies for AML has achieved fewer breakthroughs, compared to those for plasma cell neoplasms and lymphoid malignancies. Studies have demonstrated interactions between ferroptosis and immune regulation in the AML microenvironment [10,11]. Preclinical studies have shown that some ferroptosis inducers may strengthen the clinical therapeutic effect of immune checkpoint inhibitors in tumors that tend to respond poorly to immunotherapy [12]. Immune checkpoint inhibitors and ferroptosis activators synergistically inhibit hepatocellular carcinoma cell proliferation. However, the mechanism underlying this has not yet been fully elucidated [13,14]. As a result, screening and validating the involvement of ferroptosis–immune related genes (FIRGs) in AML prognosis and treatment sensitivity is important.

The present study aimed to identify differential FIRGs in patients with AML. A risk score model on the foundation of five FIRGs was constructed to forecast the AML prognosis. Finally, the potential therapeutic value of the risk assessment model was determined. Our findings could have clinical implications for the prognosis and treatment of AML.

2. Materials and methods

2.1. Data collection from public databases

The transcriptomic data of 129 samples from patients with AML with both clinical and information on survival were acquired from The Cancer Genome Atlas (TCGA) database (https://portal.gdc.cancer.gov/). TCGA-LAML cohort was used as the training dataset. Two validation datasets, both generated on the GPL96 platform, were acquired from the Gene Expression Omnibus (GEO) database (https://www.ncbi.nlm.nih.gov/geo/). The transcriptome data and survival information for 162 and 417 AML samples were obtained from GSE12417 and GSE37642, respectively. The GSE164894 data set was used to compare the risk score between AML patients who did and did not achieve complete remission (CR). The GSE60926 data set was further used to compare the risk scores between acute lymphoblastic leukemia patients with and without central nervous system (CNS) involvement. Principal component analysis (PCA) analysis was employed during exploratory data analysis (EDA) [15].

2.2. Assessment of ferroptosis-related enrichment score

FIRGs were retrieved from the MsigDB data base (http://www.gsea-msigdb.org/gsea/msigdb/) and FerrDb data base (http://www.zhounan.org/ferrdb/). After merging and de-duplication, 275 FIRGs were identified. The ferroptosis-related enrichment score (ferroptosis score) for each AML sample in the TCGA-LAML dataset was calculated using single sample gene set enrichment analysis (ssGSEA) [16,17]. The optimal cutpoint was obtained with the surv_cutpoint function from the R package 'survminer' (v0.4.9) based on the ferroptosis score of each sample [18]. The 129 AML patients from TCGA database were then separated into high- and low-ferroptosis score groups based on the cutpoint. To compare the differences in survival of the high- and low-ferroptosis scoring groups, Kaplan-Meier (K-M) analysis and log-rank testing were used [19]. Furthermore, to validate the relationship between the ferroptosis enrichment score and ferroptosis, differential expression of ferroptosis signal pathway marker genes was analyzed in the two groups. Genes involved in the ferroptosis pathway were obtained from the Kyoto Encyclopedia of Genes and Genomes (KEGG) database (https://www.kegg.jp/; map04216).

2.3. Identification of FIRGs

The 'limma' R package was used to identify differentially expressed genes (DEGs) between two ferroptosis score groups in the TCGA dataset [20]. The cutpoint for DEGs was P-value < 0.05 and log2 fold change |(FC)| > 1. To visualize the variations in genetic expression levels between the two groups, a Volcano plot was created. The expression of the top 50 DEGs was depicted in a heat map. The ImmPort database (https://www.immport.org/home) yielded a total of 1793 genes related to

immunity. A Venn diagram between DEGs and 1793 immune related genes were used to identify FIRGs.

2.4. Functional and pathway enrichment analyses of FIRGs

The 'clusterProfiler' program was adopted to perform gene ontology (GO) enrichment as well as KEGG pathway analyses on the FIRGs to explore the common functions and pathways [21]. Biological processes (BP), cellular components (CC), and molecular functions (MF) linked to FIRGs were mainly defined using GO enrichment analysis. The biological pathways associated with FIRGs were discovered using KEGG pathway analysis. The *P*-value threshold for enrichment significance was adjusted to 0.05.

2.5. Construction and validation of the prognostic risk score model

To find FIRGs that were substantially linked with the OS of AML patients in the training sample, univariable Cox regression analyses were used. To detect FIRG signatures and determine their respective coefficients value, LASSO regressive analyses of candidate FIRGs were performed [22,23]. Using the 'glmnet' R package [24], a tenfold cross verification was utilized to find optimal values for the alpha and lambda parameters. The following equation was introduced to calculate the risk score: Risk score = $\beta 1X1 + \beta 2X2 + \ldots + \beta nXn$, where β refers to the regressive coefficient and X1 denotes the genetic expression level. The median risk score was computed via the 'survminer' program in R program to separate AML patients into high-risk and low-risk groups. The K-M analysis and log-rank test were then employed to contrast the OS of the two groups. The K-M 'survival ROC' program in R software was employed to plot receiver operating characteristic (ROC) curves and measure the area under the ROC curve (AUC) values to predictive efficiency of the risk model. Better efficiency was indicated by larger AUC value [25]. In addition, a risk plot was created with R software's 'pheatmap' package [26]. The effectiveness of the risk scoring model in distinguishing the high-risk group from the low-risk group was further assessed via t-distributed stochastic neighbor embedding (t-SNE) analyses [27]. This approach was used to validate both GSE12417 and GSE37642 datasets. Moreover, integrated discrimination improvement (IDI) analysis was performed to compare the overall improvement of the risk prediction models [28–30].

2.6. Independent prognostic analysis and construction of a nomogram

Univariable regression and multivariable Cox regression analyses were performed to find independent prediction factors of OS in the TCGA-LAML dataset. Using the R packages 'rms' and 'nomogramEx' [11], a nomogram including the risk scoring and clinicopathological parameters was created. Corresponding and correction curves of 1-, 3- , and 5-year OS were constructed with the 'regplot' R package to further verify the accuracy of this nomogram [31]. Decision curve analysis (DCA) curves at 3 and 5 years were also drawn to evaluate the prognostic model [32].

2.7. Immune infiltration analysis by ssGSEA

The ssGSEA was introduced to determine the enrichment score of 24 immunocytes [33]. A box plot was drawn to visualize the differences in infiltration of 24 immune cell types between the low-

and high-risk groups. Associations between the prognostic model genes and differential immune cells were analyzed using Spearman's correlation analysis. Correlation coefficient |cor| > 0.3 and *P*-value < 0.05 were considered statistically significant.

2.8. Assessment of the immunotherapeutic and chemotherapeutic responses

Based on the half-maximal inhibitory concentration (IC50) reported for every patient on the Genomics of Drug Sensitivity in Cancer web site, the 'pRRophetic' R package was employed to study the chemotherapeutic response [34]. In addition, an unsupervised subclass mapping method (SubMap) was applied to predict response to anti-programmed cell death ligand 1 (PD1) and anti-cytotoxic T-lymphocyte associated protein 4 (CTLA4) immunotherapy. A data file containing 47 cutaneous melanoma samples and expression data of 791 genes was obtained from a prior study [35]. The R package 'pheatmap' was utilized to visualize these findings.

2.9. Statistical analyses

The R programming language was used for all studies. The function and references for R packages are listed in Table S1. Data from multiple groups were compared employing the t-test, Wilcoxon rank-sum test, Kruskal-Wallis H test, and Chi-square test. If not specified above, a *P*-value less than 0.05 was considered statistically significant.

3. Results

3.1. Establishment and validation of ferroptosis score

The transcriptome data and clinical features of the patients with AML were acquired from the TCGA and GEO databases. The TCGA-LAML cohort was chosen as the training dataset. GSE12417 and GSE37642 were the validation datasets. Table S2 provides details on clinical characteristics of the training dataset and two validation datasets. Exploratory data analysis of the TCGA-LAML cohort revealed no major changes in the global gene expression of AML patients with various survival statuses or durations (Figure S1).

The workflow for the study is shown in Figure 1. The study included 129 AML patients identified from the TCGA database. The ferroptosis score of every sample was obtained by ssGSEA. Using the median ferroptosis score as the threshold, all AML cases were separated into a high-ferroptosis score group and a low-ferroptosis score group. The OS of the low-ferroptosis group was superior to that of the high-ferroptosis group (median OS, 66 vs. 25.3 months, $P < 0.05$; Figure 2A). Furthermore, the differences in gene expression of biomarkers involved in ferroptosis signaling between two groups were assessed. The expression of 11 genes (*ATG3, ATG5, GCLC, GCLM, GPX4, LPCAT3, PCBP1, PRNP, SAT1, SLC3A2, and SLC39A8*) was substantially different between the two groups. These findings suggested a significant association between the predicted ferroptosis score and ferroptosis in patients with AML (Figure S2).

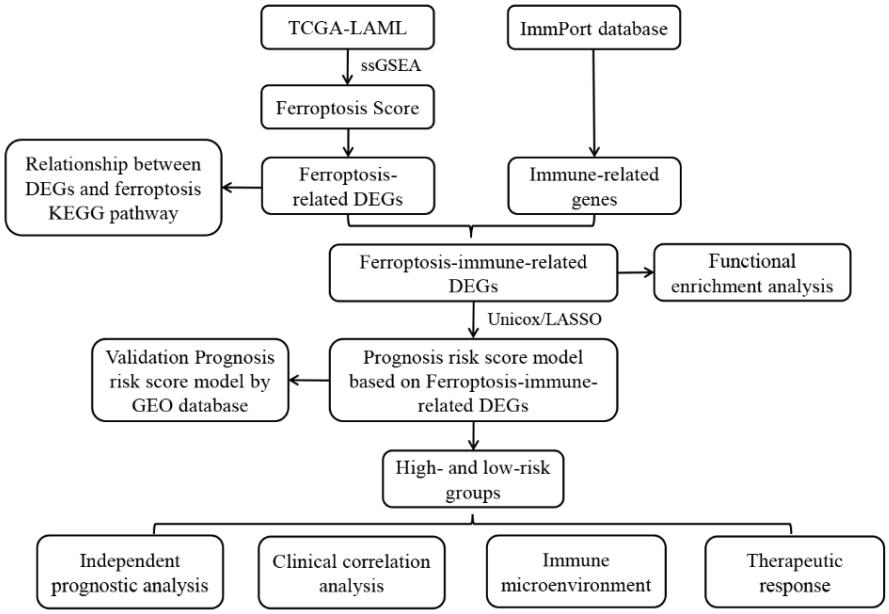

Figure 1. Schematic diagram of the study workflow.

3.2. Identification of FIRGs and functional enrichment analyses

Limma software was adopted to examine genetic expression changes between two groups. The 1061 DEGs in the groups (Figure 2B, Figure S3, Table S3) included 104 downregulated DEGs and 957 upregulated DEGs. Using the intersection of DEGs and immunity-related genes, 157 FIRGs were discovered (Figure 2C, Table S4).

The FIRGs were examined by GO and KEGG enrichment analysis. GO analysis of BP revealed that FIRGs were most enriched in immune response, leukocyte chemotaxis, and phagocytosis. In terms of CC, the FIRGs were highly enhanced on the outer surface of the plasma membrane. Regarding MF, FIRGs were enriched in signaling receptor activator and cytokine and chemokine activity, in addition to receptor binding. The top ten enrichment results for each GO category are illustrated in Figure 2D. KEGG pathway enrichment results revealed that the FIRGs were remarkably enriched in cytokine-cytokine receptor interplay, chemotactic factor signal path, neutrophil extracellular trap formation, phagosome, and signaling pathways for tumor necrosis factor (TNF), interleukin (IL)-17, mitogen-activated protein kinase, nuclear factor-kappa B (NF-κB), and Toll-like receptor (TLR) (Figure 2E).

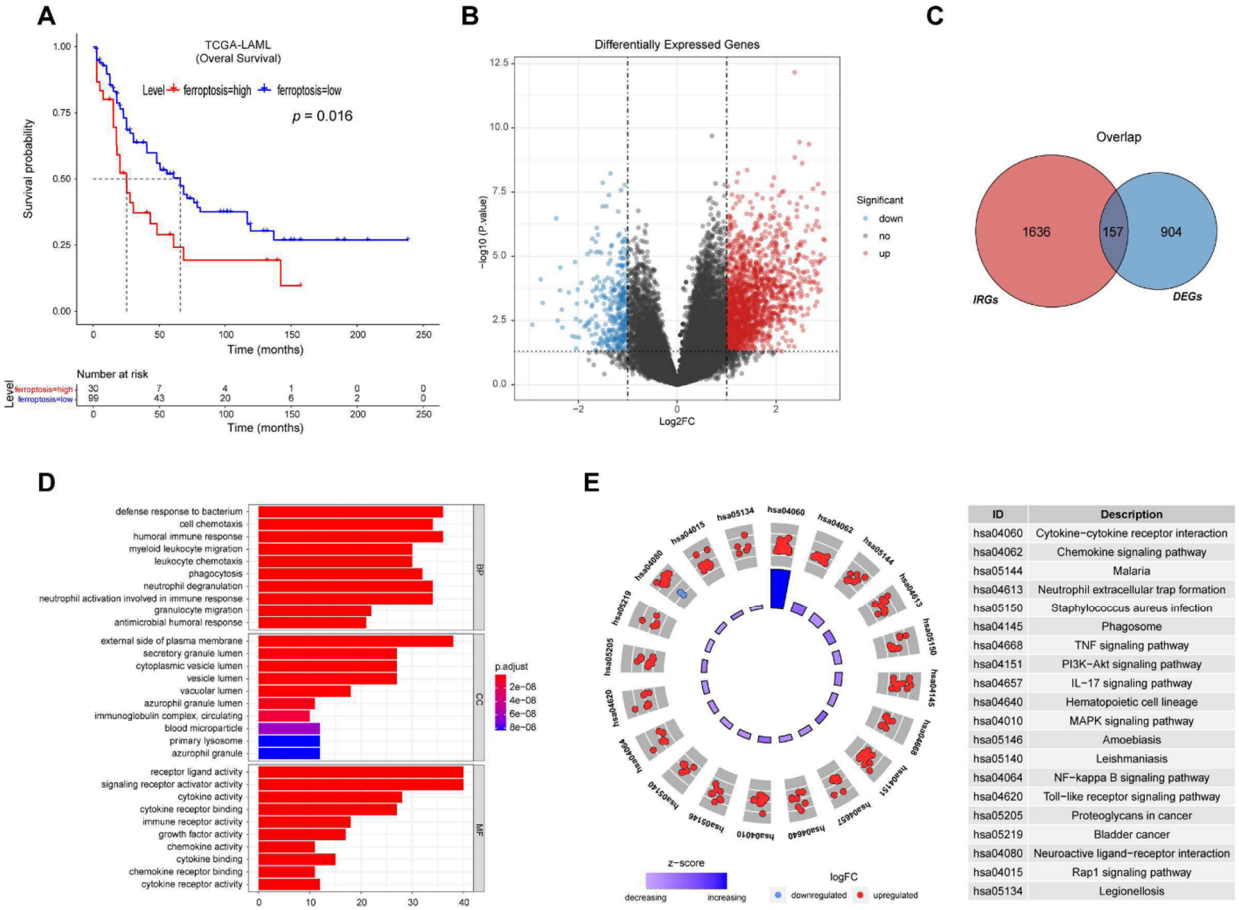

ID	Description
hsa04060	Cytokine−cytokine receptor interaction
hsa04062	Chemokine signaling pathway
hsa05144	Malaria
hsa04613	Neutrophil extracellular trap formation
hsa05150	Staphylococcus aureus infection
hsa04145	Phagosome
hsa04668	TNF signaling pathway
hsa04151	PI3K−Akt signaling pathway
hsa04657	IL−17 signaling pathway
hsa04640	Hematopoietic cell lineage
hsa04010	MAPK signaling pathway
hsa05146	Amoebiasis
hsa05140	Leishmaniasis
hsa04064	NF−kappa B signaling pathway
hsa04620	Toll−like receptor signaling pathway
hsa05205	Proteoglycans in cancer
hsa05219	Bladder cancer
hsa04080	Neuroactive ligand−receptor interaction
hsa04015	Rap1 signaling pathway
hsa05134	Legionellosis

Figure 2. Screening of FIRGs and functional enrichment analysis. (A) K-M analysis of OS for patients in high- and low-ferroptosis score groups. (B) Volcano plot of differentially expressed FIRGs. Red dots indicate upregulated DEGs, green dots indicate downregulated DEGs, and black dots indicate genes that were not differentially expressed. (C) Venn diagram of FIRGs and immunity-associated genes. (D) GO and (E) KEGG enrichment analyses for FIRGs.

3.3. Establishment and verification of five-gene prognosis risk score model based on FIRGs

The prognostic significance of the FIRGs was evaluated using univariable Cox regression analyses on the training set. Thirty-three FIRGs were significantly associated with the OS of AML patients ($P < 0.05$; Figure 3A). To construct a prognosis model, these 33 FIRGs were further included in a LASSO regression analysis. Five FIRGs (*BMP2, CCL3, EBI3, ELANE*, and *S100A6*) were screened (Figure 3B, C). The risk scoring was calculated according to the expression levels and regression coefficients as: risk score = 0.01394 × BMP2 + 0.07846 × CCL3 + 0.11465 × EBI3 + (−0.0783) × ELANE + 0.16425 × S100A6. Based on the average risk score, AML patients were divided into high- and low-risk groups. Based on the five-gene prognostic model, Figure 4J shows risk score distribution, OS results, and model gene expressions in the two risk groups. Patients in the high-risk group had lower survival durations than patients in the low-risk group. Reduced expression of *ELANE* and increased expression of the other four genes were linked to higher risk. As indicated in Figure 4A, high-risk patients had a much lower OS in contrast to low-risk patients (median OS, 27.9 vs. 116.8 months, $P < 0.001$). Time-dependent ROC curves were constructed to illustrate predictive performance. In the training set, the

1-, 3-, and 5-year AUC was 0.698, 0.763, and 0.776, respectively, indicating good efficiency (Figure 4D). Meanwhile, t-SNE analysis confirmed that the patients in the two risk groups had been allocated (Figure 4G). The collective findings demonstrated that the constructed model performed well in predicting OS of patients with AML.

We computed the risk scores of individuals in the GSE12417 and GSE37642 datasets to verify the dependability of the constructed model. The outcomes of the two validation sets' analyses were consistent with those of the TCGA cohort. The high-risk group in GSE12417 also exhibited a low survival rate (Figure 4B, K), with an AUC > 0.6 in the ROC curve at 1, 3, and 5 years (Figure 4E). The t-SNE analysis illustrated that the patient distributions in these two groups were remarkably diverse (Figure 4H). The risk model validation results from dataset GSE37642 were consistent with those from GSE12417 (Figure 4C, F, I, and L). The results of the analyses of the two validation sets matched the results from the TCGA cohort. Furthermore, we compared our risk score model to risk models utilized in prior AML studies (PMID: 35111195; PMID: 35359394), as identified by the IDI. The discrimination of our model was higher than that of two recently reported models (the model in PMID 35111195: IDI 10.2%; 95% CI: 3.7 to 16.5%; $P = 0.018$; the model in PMID 35359394: IDI 10.2%; 95% CI: 3.2 to 16.1%; $P = 0.016$). The results indicated that our risk model significantly improved predictive accuracy (Figure S4). The five-gene prognostic model could successfully forecast the OS of patients with AML.

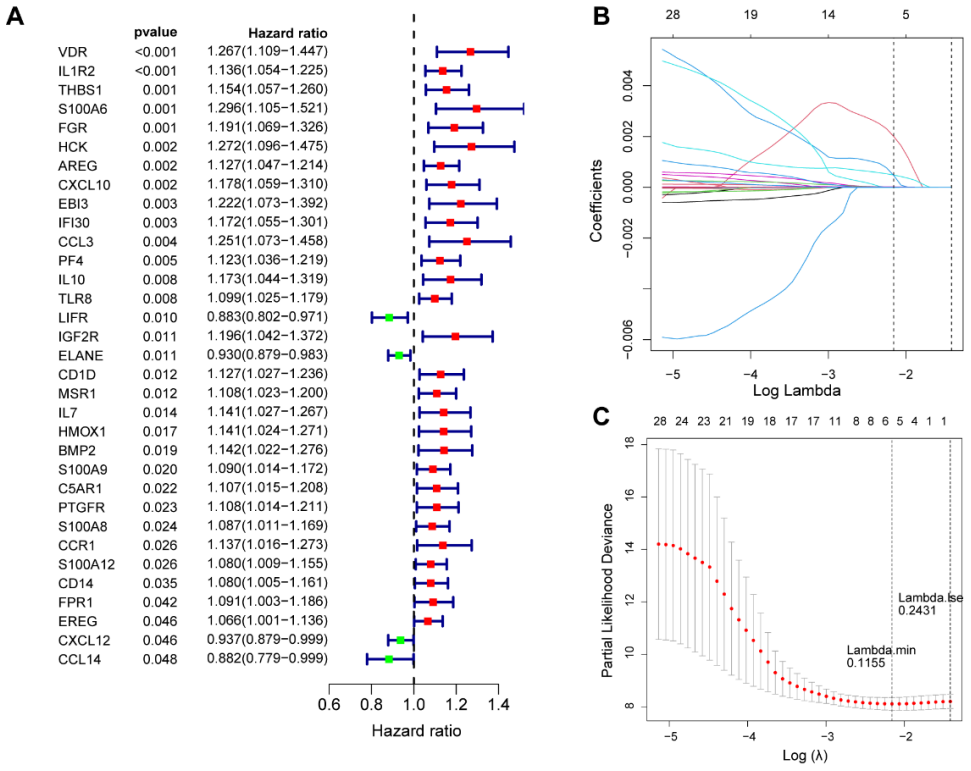

Figure 3. Establishment and evaluation of a prognosis risk score model. (A) Forest plots of FIRGs by univariate Cox regression analysis. (B and C) Construction of prognostic gene signature by LASSO regression analysis.

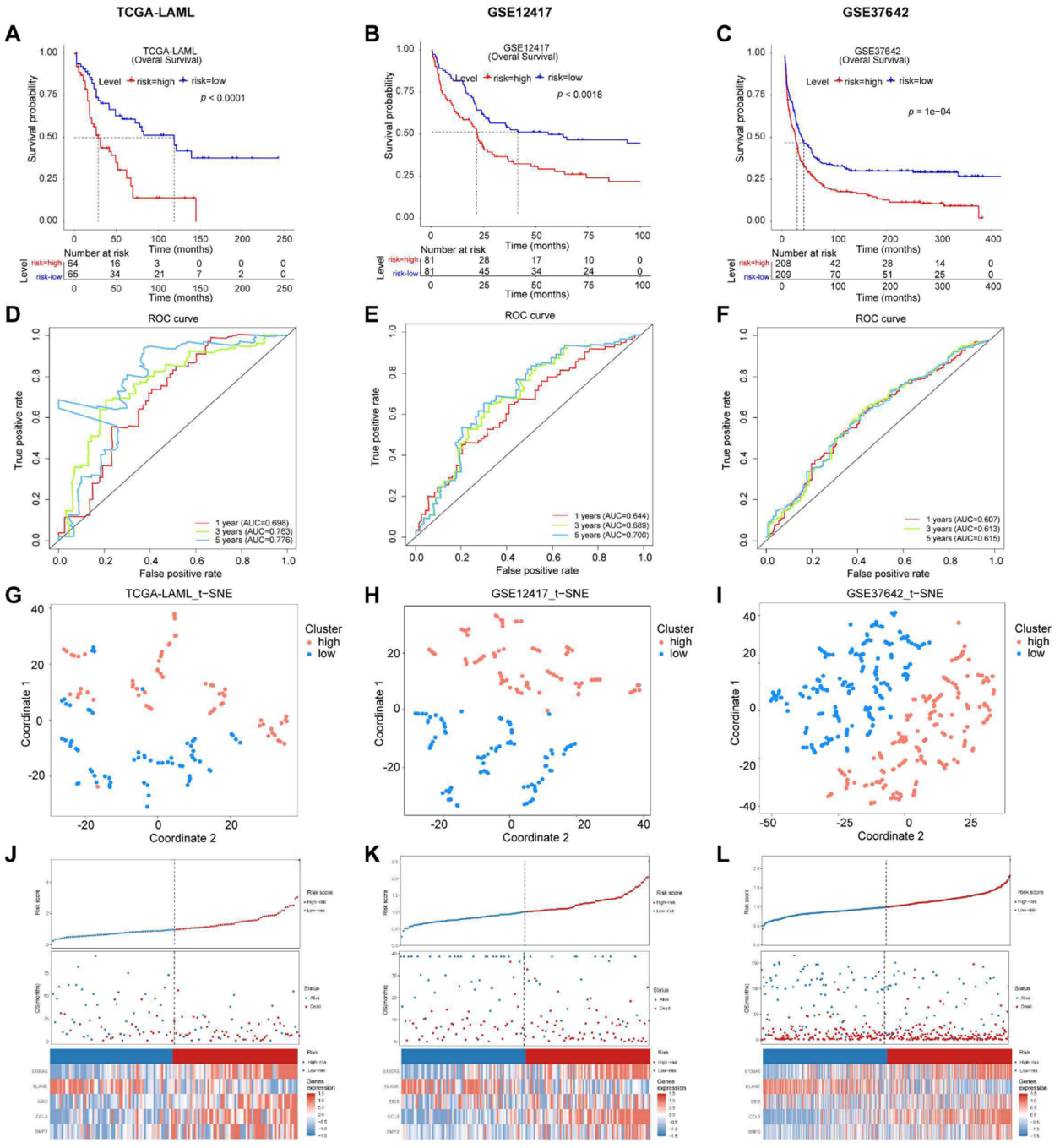

Figure 4. Validation of the prognosis risk score model in TCGA-LAML and two GEO cohorts. K-M survival curve of OS for individuals in high-risk and low-risk groups in (A) TCGA-LAML, (B) GSE12417, and (C) GSE37642. Time-dependent ROC curve analysis for 1-, 3-, and 5-year OS of the model in (D) TCGA-LAML, (E) GSE12417, and (F) GSE37642. Results of t-SNE analysis verifying the ability of the model to classify two groups in (G) TCGA-LAML, (H) GSE12417, and (I) GSE37642. Risk score distribution, OS, and gene expression in (J) TCGA-LAML, (K) GSE12417, and (L) GSE37642.

Table 1. Clinical characteristics for patients in high- and low-risk groups of TCGA-LAML cohort.

	Total	High-risk	Low-risk	*P*-value
age(year)				
Mean (SD)	53.5 (± 16.3)	58.5 (± 15.3)	48.6 (± 15.9)	< 0.001
>60	55 (42.6%)	36 (56.3%)	19 (29.2%)	0.003
<=60	74 (57.4%)	28 (43.8%)	46 (70.8%)	
Gender				
Female	60 (46.5%)	27 (42.2%)	33 (50.8%)	0.38
Male	69 (53.5%)	37 (57.8%)	32 (49.2%)	
Race				
ASIAN	1 (0.8%)	1 (1.6%)	0 (0.0%)	0.64
BLACK OR AFRICAN AMERICAN	10 (7.9%)	4 (6.2%)	6 (9.5%)	
WHITE	116 (91.3%)	59 (92.2%)	57 (90.5%)	
WBC (10^9/L)				
Mean (SD)	31.6 (± 37.5)	35.0 (± 37.2)	28.2 (± 37.8)	0.26
<=100	118 (91.5%)	58 (90.6%)	60 (92.3%)	0.715
>100	8 (6.2%)	5 (7.8%)	3 (4.6%)	
HB(g/dL)				
Mean (SD)	9.6 (± 1.4)	9.3 (± 1.2)	9.8 (± 1.5)	0.056
Platelet(10^9/L)				
Mean (SD)	66.1 (± 55.3)	66.0 (± 58.3)	66.1 (± 52.7)	0.87
Peripheral blasts (%)				
Mean (SD)	37.8 (± 30.9)	33.0 (± 30.1)	42.7 (± 31.1)	0.088
Bone marrow blasts (%)				
Mean (SD)	68.3 (± 19.6)	67.4 (± 20.6)	69.2 (± 18.7)	0.56
FAB subtype				
M0	12 (9.3%)	6 (9.4%)	6 (9.2%)	< 0.001
M1	31 (24.0%)	19 (29.7%)	12 (18.5%)	
M2	31 (24.0%)	9 (14.1%)	22 (33.8%)	
M3	14 (10.9%)	1 (1.6%)	13 (20.0%)	
M4	26 (20.2%)	17 (26.6%)	9 (13.8%)	
M5	12 (9.3%)	9 (14.1%)	3 (4.6%)	
M6	2 (1.6%)	2 (3.1%)	0 (0.0%)	
M7	1 (0.8%)	1 (1.6%)	0 (0.0%)	
OS (months)				
Mean (SD)	52.1 (± 50.4)	34.7 (± 32.8)	69.2 (± 58.5)	< 0.001
Vital				
Alive	51 (39.5%)	17 (26.6%)	34 (52.3%)	0.004
Dead	78 (60.5%)	47 (73.4%)	31 (47.7%)	

3.4. Association between risk score model and clinicopathological features

We explored the associated clinical data of patients with AML in TCGA to determine the

association between the model and clinicopathology traits. The analysis revealed that the risk scoring differed significantly between age groups, FAB subtypes, and OS (Table 1). Stratification analysis revealed the prognosis signature as a promising predictor of survival of the AML clinical subtypes. In addition, the CR rate in the high- and low-risk patients was explored. Patients who achieved CR appeared to have lower risk score compared to the patients without CR, but there was no statistical significance between the two groups (Figure S5A). Low-risk patients seemed to achieve non-significantly higher CR rates than high-risk patients (Figure S5B). We then investigated the relationship between CNS involvement and risk score in acute lymphoblastic leukemia patients. As shown in Figure S6A, these patients displayed significantly higher risk score than patients without CNS leukemia. Patients with high-risk had a higher proportion of CNS leukemia (Figure S6B). The result has a potential reference value for exploring the rate of CNS leukemia in different risk score groups of AML patients.

3.5. Risk factor as an independent prognostic factor and nomogram construction

Univariable and multivariable Cox regression analyses were performed to explore if risk scoring could be considered a prognostic factor for individuals with AML independent of other clinical variables. Age, ferroptosis group, and risk score were all linked to patient prognosis in the univariate analysis (Figure 5A). The risk score might be utilized to predict patient prognosis independently, according to the multivariate Cox regression analysis (Figure 5B). In multivariate analysis, age was also a significant prognostic factor.

The independent prognostic factors of age and risk score were used to create a nomogram to forecast 1-, 3-, and 5-year OS (Figure 5C). The nomogram's C-index was 0.680. Calibration plots revealed that the nomogram succeeded in predicting the three survival probabilities in AML patients (Figure 5D). DCA of the risk model and nomogram was then performed to assess the prediction effectiveness (Figure S7A, B).

3.6. Comparison of immune infiltration between two risk groups

Next, ssGSEA was used to calculate the percentage of 24 immune cells in the two groups. Low-risk patients had more T helper and Th2 cells than high-risk patients (Figure 6A). In comparison to the low-risk group, the high-risk group had considerably more activated dendritic cells (aDCs), $CD8^+$ T cells, cytotoxic T cells, induced DCs (iDCs), neutrophils, macrophages, natural killer (NK) CD56dim cells, NK CD56bright cells, Th17 cells, Th1 cells, T follicular helper cells (TFHs), and regulatory T cells (Treg). These results suggested that the immunological milieu of the two risk groups was significantly different. The Pearson correlation between different immune cells and prognostic genes was then examined (Figure 6B). S100A6 was found to have a strong relationship with iDCs, macrophages, and neutrophils. T helper cell levels of chemokine (C-C motif) ligand 3 (CCL3) and S100A6 exhibited a significant negative correlation. TFH, Th1 cells, macrophages, Tgd, neutrophils, NK CD56bright cells, and iDCs were also correlated with bone morphogenetic protein 2 (BMP2). CCL3 was linked to macrophages, iDC, neutrophils, NK CD56bright cells, NK CD56dim cells, Th17 cells, Th1 cells, and TFH cells. A substantial positive connection was found between Epstein-Barr virus-induced gene 3 (EBI3) and aDCs, NK CD56dim cells, TFHs, and macrophages.

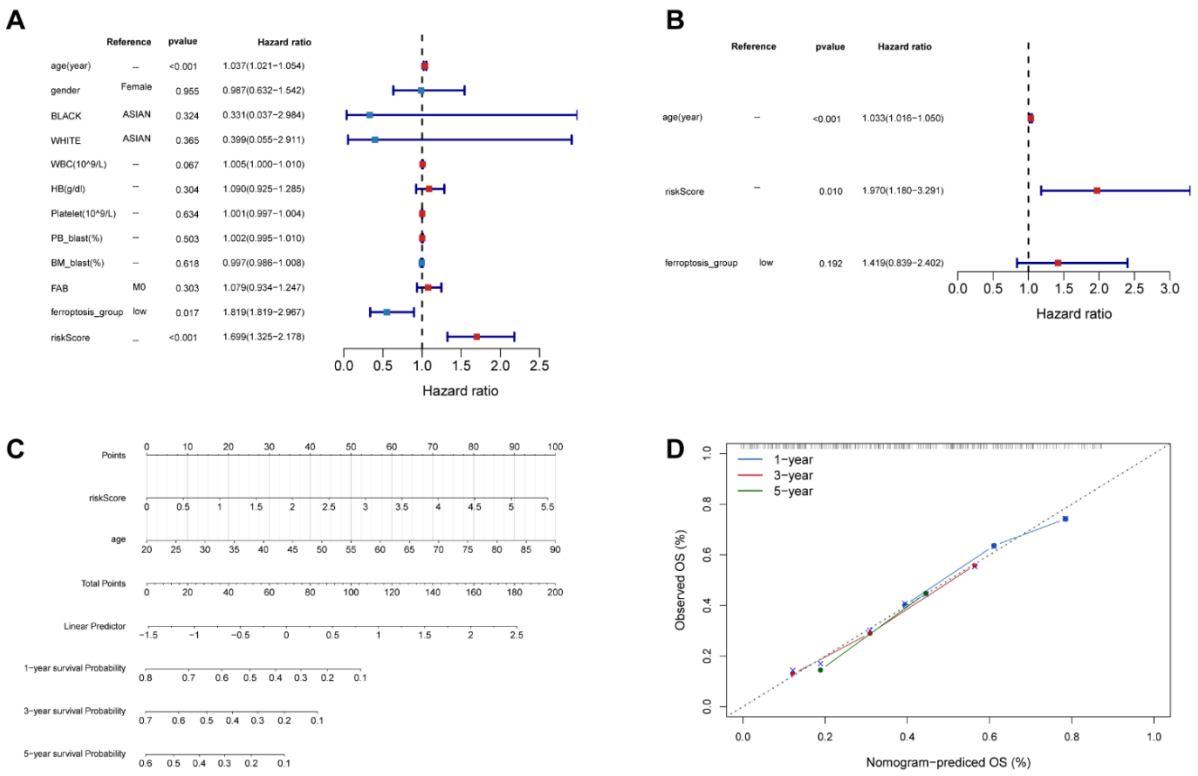

Figure 5. Independent prognosis value of the five-gene signature and creation of a nomograph. (A and B) Forest plots of risk scores and other clinical features with univariable (A) and multivariable (B) Cox regressive analysis. (C) Nomogram created to forecast the OS of AML patients. (D) The nomogram calibration curves of survival probabilities.

3.7. The five-gene prognostic risk model predicts the sensitivity to chemotherapy and immunotherapy

The SubMap algorithm was utilized to predict the clinical activity of immune checkpoint inhibitors in the two risk groups (Figure 6C). The high-risk group was more responsive to anti-PD-1 immunotherapy ($P < 0.05$). In addition, using drug sensitivity data obtained from the Genomics of Drug Sensitivity in Cancer website, we estimated the chemosensitivity of the two groups to 133 drugs. High-risk patients had larger IC50 values for midostaurin (a multitargeted kinase inhibitor), NSC 87877 (inhibitor of Src homology-2 domain-containing protein tyrosine phosphatase-2), and pyrimethamine (inhibitor of dihydrofolate reductase) (Figure 6D). The findings indicate the value of the five-gene prognostic risk model in predicting treatment sensitivity to immunotherapy and targeted therapy.

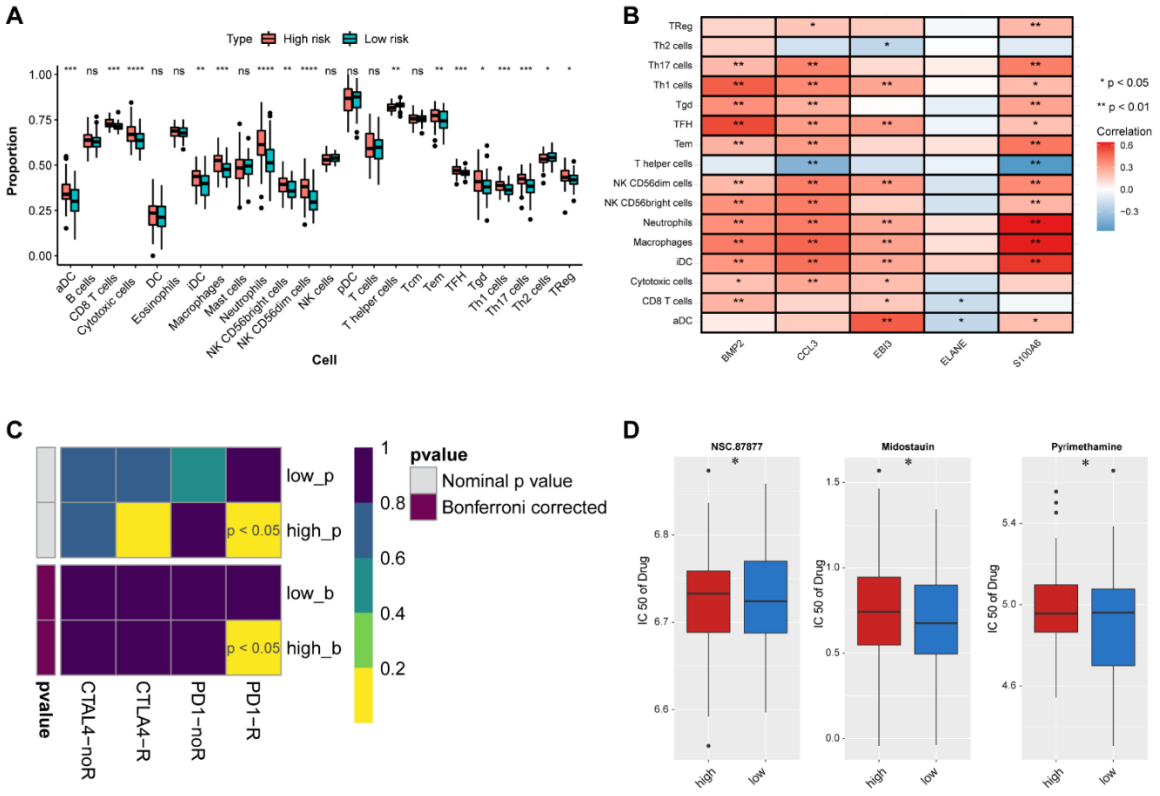

Figure 6. Assessment of the correlations between the risk score model and immune infiltration and therapeutic sensitivity. (A) Immune infiltration analysis between two risk groups. (B) The Pearson correlation between different immune cells and prognostic genes. (C) Immunotherapeutic responses to anti-PD1 and anti-CTLA4 treatments. (D) Sensitivity analysis of chemotherapeutic response based on IC50. * $P < 0.01$.

4. Discussion

An accurate prognostic signature in patients with AML might help guide individualized treatment plans and improve therapeutic efficacy [36]. Ferroptosis is an iron-dependent form of cell death driven by the increase of lipid peroxidation to fatal levels. There is growing interest regarding the interaction between ferroptosis and AML treatments [37]. Furthermore, ferroptosis affects the tumor immune microenvironment and potentially influences the outcome of immunotherapy [38,39]. Comprehensive research of the role of FIRGs in AML prognosis may reveal new avenues in the prediction of patient prognosis.

We used ssGSEA to determine the ferroptosis-related enrichment scores for each TCGA-LAML sample with a collection of known ferroptosis-related genes. The samples were subsequently separated into high- and low-ferroptosis score groups, with significant DEGs identified in the two groups. This method may provide theoretical support for the discovery of novel ferroptosis-related genes. Intersecting the DEGs with immune related genes identified 157 FIRGs. Functional enrichment analysis revealed that 157 FIRGs were enriched in the TNF, phosphoinositide 3-kinase (PI3K)-Akt, and IL-17 signaling pathways. These three pathways are associated with AML pathogenesis. In AML patients, abnormally elevated TNF-α levels could promote Treg cell development through the TNF-α–

TNFR2 pathway, thus aggravating the progression of AML [40]. Furthermore, abnormal activation of the PI3K-Akt or IL-17 pathway is also linked with discouraging prognosis in AML [41,42].

We analyzed prognosis-related FIRG signatures in patients with AML. Through univariate Cox and LASSO regression analyses, five signature genes (*BMP2*, *CCL3*, *EBI3*, *ELANE*, and *S100A6*) were screened for the prognostic risk score model. Among them, *BMP2*, *CCL3*, and *EBI3* are related to the progression and recurrence of AML. For example, previous studies implicated *BMP2* in the promotion of stemness maintenance and self-renewal in leukemia stem cells, causing drug resistance and recurrence of AML [43,44]. *CCL3* is a poor prognostic factor for AML, and elevated *CCL3* in the leukemic environment suppresses erythropoiesis [45]. *EBI3* participates in the formation of IL-35, which can contribute to an immunosuppressive AML microenvironment and facilitate immune escape of leukemic cells [46,47]. In addition, *ELANE* and *S100A6* may also be associated with other hematopoietic malignancies [48]. Their roles in AML deserves further study.

The present study discovered that individuals with high-risk scores have poor prognosis, which is consistent with the prognostic effect of models based only on ferroptosis-related genes [29]. External validation confirmed the efficacy of this risk model in predicting the survival of AML patients. Importantly, the model was verified as an independent factor for OS in individuals with AML in both univariable and multivariable Cox regression analyses. To forecast the survival of individuals with AML, we developed a nomogram and assessed the validity of independent prognostic factors. Despite these accomplishments, further studies are required to verify the prognostic importance of the ferroptosis-immune related risk score.

We also investigated the association between the risk score model and immunocyte infiltration as well as therapeutic sensitivity to understand more about the implications of the model for AML therapy. The high-risk score group showed higher infiltration of Treg, Th17, and $CD8^+$ T cells. Tregs facilitate immune escape of AML, further promoting disease progression and relapse [49,50]. Treg cells inhibit effector T cells through direct and indirect mechanisms, including the secretion of immunosuppressive cytokines, increased ATP hydrolysis, and increased adenosine production [51–53]. The levels of Th17 cells and their related cytokines (IL-17, IL-1 β, and IL-6) are increased in newly diagnosed and incomplete remission patients with AML, suggesting that Th17 cells may be involved in the pathogenesis of AML [54]. This was confirmed by the significant enrichment of FIRGs in the IL-17 pathway, as discussed previously. Notably, we presently observed that the high-risk group had a higher $CD8^+$ T cells infiltration than the low-risk group. Although $CD8^+$ T cells are crucial effector cells involved in the killing of cancerous cells, their function may be suppressed by AML blasts [55]. The sensitivity of different risk score groups to chemotherapy and immunotherapy was also investigated. Anti-PD-1 treatment produced a higher response rate in the high-risk group. PD-1/PD-L1 inhibitors have been previously demonstrated to fully restore the functional activity of pre-existing intratumoral tumor-infiltrating lymphocytes [55,56]. Therefore, we speculated that PD-1 therapy may be important in the recovery of immune function of immunosuppressed $CD8^+$ T cells in patients with AML with a high-risk score. The low-risk group appeared to be more sensitive to midostaurin, NSC 87877, and pyrimethamine treatments. Our findings suggest that a risk score model based FIRGs is able to forecast therapeutic sensitivity and could help clinicians make more personalized treatment decisions.

5. Conclusions

A prognostic risk score model was constructed and validated based on five ferroptosis–immune

associated genes to accurately predict OS of AML patients. This risk score model could provide a basis for optimizing individualized clinical treatments.

Acknowledgments

We thank Dr. Yu-chen Li (Nanjing Agricultural University) and Dr. Sen-lin Ji (Affiliated Drum Tower Hospital, Nanjing University) for the help in our data analysis.

Conflict of interest

The authors declare that they have no known competing financial interests or personal relationships that could have appeared to influence the work reported in this paper.

References

1. K. Sasaki, F. Ravandi, T. M. Kadia, C. D. DiNardo, N. J. Short, G. Borthakur, et al., De novo acute myeloid leukemia: A population-based study of outcome in the United States based on the Surveillance, Epidemiology, and End Results (SEER) database, 1980 to 2017, *Cancer*, **127** (2021), 2049–2061. https://doi.org/10.1002/cncr.33458
2. C. Ganzel, Z. Sun, L. D. Cripe, H. F. Fernandez, D. Douer, J. M. Rowe, et al., Very poor long-term survival in past and more recent studies for relapsed AML patients: The ECOG-ACRIN experience, *Am. J. Hematol.*, **93** (2018), 1074–1081. https://doi.org/10.1002/ajh.25162
3. S. J. Dixon, K. M. Lemberg, M. R. Lamprecht, R. Skouta, E. M. Zaitsev, C. E. Gleason, et al., Ferroptosis: an iron-dependent form of nonapoptotic cell death, *Cell*, **149** (2012), 1060–1072. https://doi.org/10.1016/j.cell.2012.03.042
4. B. Hassannia, P. Vandenabeele, T. V. Berghe, Targeting ferroptosis to iron out cancer, *Cancer Cell*, **35** (2019), 830–849. https://doi.org/10.1016/j.ccell.2019.04.002
5. C. Liang, X. Zhang, M. Yang, X. Dong, Recent progress in ferroptosis inducers for cancer therapy, *Adv. Mater.*, **31** (2019), e1904197. https://doi.org/10.1002/adma.201904197
6. F. Zhang, H. Liu, Identification of ferroptosis-associated genes exhibiting altered expression in pulmonary arterial hypertension, *Math. Biosci. Eng.*, **18** (2021), 7619–7630. https://doi.org/10.3934/mbe.2021377
7. R. Birsen, C. Larrue, J. Decroocq, N. Johnson, N. Guiraud, M. Gotanegre, et al., APR-246 induces early cell death by ferroptosis in acute myeloid leukemia, *Haematologica*, **107** (2022), 403–416. https://doi.org/10.3324/haematol.2020.259531
8. D. S. Liu, C. P. Duong, S. Haupt, K. G. Montgomery, C. M. House, W. J. Azar, et al., Inhibiting the system xC(-)/glutathione axis selectively targets cancers with mutant-p53 accumulation, *Nat. Commun.*, **8** (2017), 14844. https://doi.org/10.1038/ncomms14844
9. H. Liu, Emerging agents and regimens for AML, *J. Hematol. Oncol.*, **14** (2021), 49. https://doi.org/10.1186/s13045-021-01062-w
10. Q. Zheng, Y. Zhao, J. Guo, S. Zhao, C. Fei, C. Xiao, et al., Iron overload promotes mitochondrial fragmentation in mesenchymal stromal cells from myelodysplastic syndrome patients through activation of the AMPK/MFF/Drp1 pathway, *Cell Death Dis.*, **9** (2018), 515. https://doi.org/10.1038/s41419-018-0552-7

11. H. Tanaka, J. L. Espinoza, R. Fujiwara, S. Rai, Y. Morita, T. Ashida, et al., Excessive reactive iron impairs hematopoiesis by affecting both immature hematopoietic cells and stromal cells, *Cells*, **8** (2019). https://doi.org/10.3390/cells8030226
12. V. D. Turubanova, I. V. Balalaeva, T. A. Mishchenko, E. Catanzaro, R. Alzeibak, N. N. Peskova, et al., Immunogenic cell death induced by a new photodynamic therapy based on photosens and photodithazine, *J. Immunother. Cancer*, **7** (2019), 350. https://doi.org/10.1186/s40425-019-0826-3
13. W. Wang, M. Green, J. E. Choi, M. Gijon, P. D. Kennedy, J. K. Johnson, et al., $CD8^+$ T cells regulate tumour ferroptosis during cancer immunotherapy, *Nature*, **569** (2019), 270–274. https://doi.org/10.1038/s41586-019-1170-y
14. D. H. Kim, W. D. Kim, S. K. Kim, D. H. Moon, S. J. Lee, TGF-beta1-mediated repression of SLC7A11 drives vulnerability to GPX4 inhibition in hepatocellular carcinoma cells, *Cell Death Dis.*, **11** (2020), 406. https://doi.org/10.1038/s41419-020-2618-6
15. M. Manzano, A. Patil, A. Waldrop, S. S. Dave, A. Behdad, E. Gottwein, Gene essentiality landscape and druggable oncogenic dependencies in herpesviral primary effusion lymphoma, *Nat. Commun.*, **9** (2018), 3263. https://doi.org/10.1038/s41467-018-05506-9
16. Y. Teng, B. Wang, D. Shang, N. Yang, Identification and validation of an immune and ferroptosis-combined index for non-small cell lung cancer, *Front. Genet.*, **12** (2021), 764869. https://doi.org/10.3389/fgene.2021.764869
17. B. Tang, R. Yan, J. Zhu, S. Cheng, C. Kong, W. Chen, et al., Integrative analysis of the molecular mechanisms, immunological features and immunotherapy response of ferroptosis regulators across 33 cancer types, *Int. J. Biol. Sci.*, **18** (2022), 180–198. https://doi.org/10.7150/ijbs.64654
18. B. N. Ostendorf, J. Bilanovic, N. Adaku, K. N. Tafreshian, B. Tavora, R. D. Vaughan, et al., Common germline variants of the human APOE gene modulate melanoma progression and survival, *Nat. Med.*, **26** (2020), 1048–1053. https://doi.org/10.1038/s41591-020-0879-3
19. N. Kim, H. K. Kim, K. Lee, Y. Hong, J. H. Cho, J. W. Choi, et al., Single-cell RNA sequencing demonstrates the molecular and cellular reprogramming of metastatic lung adenocarcinoma, *Nat. Commun.*, **11** (2020), 2285. https://doi.org/10.1038/s41467-020-16164-1
20. M. E. Ritchie, B. Phipson, D. Wu, Y. Hu, C. W. Law, W. Shi, et al., limma powers differential expression analyses for RNA-sequencing and microarray studies, *Nucleic Acids Res.*, **43** (2015), e47. https://doi.org/10.1093/nar/gkv007
21. G. Yu, L. G. Wang, Y. Han, Q. Y. He, clusterProfiler: an R package for comparing biological themes among gene clusters, *OMICS*, **16** (2012), 284–287. https://doi.org/10.1089/omi.2011.0118
22. N. Simon, J. Friedman, T. Hastie, R. Tibshirani, Regularization paths for cox's proportional hazards model via coordinate descent, *J. Stat. Softw.*, **39** (2011), 1–13. https://doi.org/10.18637/jss.v039.i05
23. R. Tibshirani, The lasso method for variable selection in the Cox model, *Stat. Med.*, **16** (1997), 385–395. https://doi.org/10.1002/(sici)1097-0258(19970228)16:4<385::aid-sim380>3.0.co;2-3
24. S. Stanley, K. Vanarsa, S. Soliman, D. Habazi, C. Pedroza, G. Gidley, et al., Comprehensive aptamer-based screening identifies a spectrum of urinary biomarkers of lupus nephritis across ethnicities, *Nat. Commun.*, **11** (2020), 2197. https://doi.org/10.1038/s41467-020-15986-3
25. Y. Wang, F. Hu, J. Y. Li, R. C. Nie, S. L. Chen, Y. Y. Cai, et al., Systematic construction and validation of a metabolic risk model for prognostic prediction in acute myelogenous leukemia, *Front. Oncol.*, **10** (2020), 540. https://doi.org/10.3389/fonc.2020.00540

26. S. Ullrich, R. Guigo, Dynamic changes in intron retention are tightly associated with regulation of splicing factors and proliferative activity during B-cell development, *Nucleic Acids Res.*, **48** (2020), 1327–1340. https://doi.org/10.1093/nar/gkz1180
27. B. Bengsch, T. Ohtani, O. Khan, M. Setty, S. Manne, S. O'Brien, et al., Epigenomic-guided mass cytometry profiling reveals disease-specific features of exhausted CD8 T cells, *Immunity*, **48** (2018), 1029–1045. https://doi.org/10.1016/j.immuni.2018.04.026
28. X. Tekpli, T. Lien, A. H. Rossevold, D. Nebdal, E. Borgen, H. O. Ohnstad, et al., An independent poor-prognosis subtype of breast cancer defined by a distinct tumor immune microenvironment, *Nat. Commun.*, **10** (2019), 5499. https://doi.org/10.1038/s41467-019-13329-5
29. Y. Song, S. Tian, P. Zhang, N. Zhang, Y. Shen, J. Deng, Construction and validation of a novel ferroptosis-related prognostic model for acute myeloid leukemia, *Front. Genet.*, **12** (2021), 708699. https://doi.org/10.3389/fgene.2021.708699
30. N. Jiang, X. Zhang, Q. Chen, F. Kantawong, S. Wan, J. Liu, et al., Identification of a Mitochondria-related gene signature to predict the prognosis in AML, *Front. Oncol.*, **12** (2022), 823831. https://doi.org/10.3389/fonc.2022.823831
31. Z. Zhang, G. Cortese, C. Combescure, R. Marshall, M. Lee, H. J. Lim, et al., Overview of model validation for survival regression model with competing risks using melanoma study data, *Ann. Transl. Med.*, **6** (2018), 325. https://doi.org/10.21037/atm.2018.07.38
32. B. Yang, J. Shen, L. Xu, Y. Chen, X. Che, X. Qu, et al., Genome-wide identification of a novel eight-lncrna signature to improve prognostic prediction in head and neck squamous cell carcinoma, *Front. Oncol.*, **9** (2019), 898. https://doi.org/10.3389/fonc.2019.00898
33. G. Bindea, B. Mlecnik, M. Tosolini, A. Kirilovsky, M. Waldner, A. C. Obenauf, et al., Spatiotemporal dynamics of intratumoral immune cells reveal the immune landscape in human cancer, *Immunity*, **39** (2013), 782–795. https://doi.org/10.1016/j.immuni.2013.10.003
34. P. Geeleher, N. J. Cox, R. S. Huang, Clinical drug response can be predicted using baseline gene expression levels and in vitro drug sensitivity in cell lines, *Genome Biol.*, **15** (2014), R47. https://doi.org/10.1186/gb-2014-15-3-r47
35. X. Lu, L. Jiang, L. Zhang, Y. Zhu, W. Hu, J. Wang, et al., Immune signature-based subtypes of cervical squamous cell carcinoma tightly associated with human papillomavirus type 16 expression, molecular features, and clinical outcome, *Neoplasia*, **21** (2019), 591–601. https://doi.org/10.1016/j.neo.2019.04.003
36. D. Fu, B. Zhang, S. Wu, Y. Zhang, J. Xie, W. Ning, et al., Prognosis and characterization of immune microenvironment in acute myeloid leukemia through identification of an autophagy-related signature, *Front. Immunol.*, **12** (2021), 695865. https://doi.org/10.3389/fimmu.2021.695865
37. Y. Yu, Y. Xie, L. Cao, L. Yang, M. Yang, M. T. Lotze, et al., The ferroptosis inducer erastin enhances sensitivity of acute myeloid leukemia cells to chemotherapeutic agents, *Mol. Cell Oncol.*, **2** (2015), e1054549. https://doi.org/10.1080/23723556.2015.1054549
38. F. Ye, W. Chai, M. Xie, M. Yang, Y. Yu, L. Cao, et al., HMGB1 regulates erastin-induced ferroptosis via RAS-JNK/p38 signaling in HL-60/NRAS(Q61L) cells, *Am. J. Cancer Res.*, **9** (2019), 730–739.
39. W. S. Yang, R. SriRamaratnam, M. E. Welsch, K. Shimada, R. Skouta, V. S. Viswanathan, et al., Regulation of ferroptotic cancer cell death by GPX4, *Cell*, **156** (2014), 317–331. https://doi.org/10.1016/j.cell.2013.12.010

40. M. Wang, C. Zhang, T. Tian, T. Zhang, R. Wang, F. Han, et al., Increased regulatory t cells in peripheral blood of acute myeloid leukemia patients rely on tumor necrosis factor (tnf)-alpha-tnf receptor-2 pathway, *Front. Immunol.*, **9** (2018), 1274. https://doi.org/10.3389/fimmu.2018.01274
41. I. Nepstad, K. J. Hatfield, I. S. Gronningsaeter, H. Reikvam, The PI3K-Akt-mTOR signaling pathway in human acute myeloid leukemia (AML) cells, *Int. J. Mol. Sci.*, **21** (2020). https://doi.org/10.3390/ijms21082907
42. Y. Han, A. Ye, L. Bi, J. Wu, K. Yu, S. Zhang, Th17 cells and interleukin-17 increase with poor prognosis in patients with acute myeloid leukemia, *Cancer Sci.*, **105** (2014), 933–942. https://doi.org/10.1111/cas.12459
43. T. A. Gruber, A. L. Gedman, J. Zhang, C. S. Koss, S. Marada, H. Q. Ta, et al., An Inv(16)(p13.3q24.3)-encoded CBFA2T3-GLIS2 fusion protein defines an aggressive subtype of pediatric acute megakaryoblastic leukemia, *Cancer Cell*, **22** (2012), 683–697. https://doi.org/10.1016/j.ccr.2012.10.007
44. F. Zylbersztejn, M. Flores-Violante, T. Voeltzel, F. E. Nicolini, S. Lefort, V. Maguer-Satta, The BMP pathway: A unique tool to decode the origin and progression of leukemia, *Exp. Hematol.*, **61** (2018), 36–44. https://doi.org/10.1016/j.exphem.2018.02.005
45. Y. Wang, A. Gao, H. Zhao, P. Lu, H. Cheng, F. Dong, et al., Leukemia cell infiltration causes defective erythropoiesis partially through MIP-1alpha/CCL3, *Leukemia*, **30** (2016), 1897–1908. https://doi.org/10.1038/leu.2016.81
46. O. Devergne, M. Birkenbach, E. Kieff, Epstein-Barr virus-induced gene 3 and the p35 subunit of interleukin 12 form a novel heterodimeric hematopoietin, *Proc. Natl. Acad. Sci. U S A*, **94** (1997), 12041–12046. https://doi.org/10.1073/pnas.94.22.12041
47. Q. Tao, Y. Pan, Y. Wang, H. Wang, S. Xiong, Q. Li, et al., Regulatory T cells-derived IL-35 promotes the growth of adult acute myeloid leukemia blasts, *Int. J. Cancer*, **137** (2015), 2384–2393. https://doi.org/10.1002/ijc.29563
48. H. Tamai, H. Yamaguchi, K. Miyake, M. Takatori, T. Kitano, S. Yamanaka, et al., Amlexanox downregulates S100A6 to sensitize KMT2A/AFF1-positive acute lymphoblastic leukemia to tnfalpha treatment, *Cancer Res.*, **77** (2017), 4426–4433. https://doi.org/10.1158/0008-5472.CAN-16-2974
49. C. Ustun, J. S. Miller, D. H. Munn, D. J. Weisdorf, B. R. Blazar, Regulatory T cells in acute myelogenous leukemia: is it time for immunomodulation?, *Blood*, **118** (2011), 5084–5095. https://doi.org/10.1182/blood-2011-07-365817
50. P. van Galen, V. Hovestadt, M. H. Wadsworth Ii, T. K. Hughes, G. K. Griffin, S. Battaglia, et al., Single-Cell RNA-Seq reveals AML hierarchies relevant to disease progression and immunity, *Cell*, **176** (2019), 1265–1281. https://doi.org/10.1016/j.cell.2019.01.031
51. M. J. Szczepanski, M. Szajnik, M. Czystowska, M. Mandapathil, L. Strauss, A. Welsh, et al., Increased frequency and suppression by regulatory T cells in patients with acute myelogenous leukemia, *Clin. Cancer Res.*, **15** (2009), 3325–3332. https://doi.org/10.1158/1078-0432.CCR-08-3010
52. X. Wang, J. Zheng, J. Liu, J. Yao, Y. He, X. Li, et al., Increased population of CD4(+)CD25(high), regulatory T cells with their higher apoptotic and proliferating status in peripheral blood of acute myeloid leukemia patients, *Eur. J. Haematol.*, **75** (2005), 468–476. https://doi.org/10.1111/j.1600-0609.2005.00537.x

53. S. F. Hausler, I. M. del Barrio, J. Strohschein, P. A. Chandran, J. B. Engel, A. Honig, et al., Ectonucleotidases CD39 and CD73 on OvCA cells are potent adenosine-generating enzymes responsible for adenosine receptor 2A-dependent suppression of T cell function and NK cell cytotoxicity, *Cancer Immunol. Immunother.*, **60** (2011), 1405–1418. https://doi.org/10.1007/s00262-011-1040-4
54. S. Yu, C. Liu, L. Zhang, B. Shan, T. Tian, Y. Hu, et al., Elevated Th22 cells correlated with Th17 cells in peripheral blood of patients with acute myeloid leukemia, *Int. J. Mol. Sci.*, **15** (2014), 1927–1945. https://doi.org/10.3390/ijms15021927
55. H. A. Knaus, S. Berglund, H. Hackl, A. L. Blackford, J. F. Zeidner, R. Montiel-Esparza, et al., Signatures of CD8+ T cell dysfunction in AML patients and their reversibility with response to chemotherapy, *JCI Insight*, **3** (2018). https://doi.org/10.1172/jci.insight.120974
56. M. Yi, D. Jiao, H. Xu, Q. Liu, W. Zhao, X. Han, et al., Biomarkers for predicting efficacy of PD-1/PD-L1 inhibitors, *Mol. Cancer*, **17** (2018), 129. https://doi.org/10.1186/s12943-018-0864-3

AIMS Press